РАЗДЕЛ ТРЕТИЙ
МАТЕРИАЛЫ РЕАКТОРОВ НА ТЕПЛОВЫХ НЕЙТРОНАХ

УДК 669.018.2

IRRADIATION-ASSISTED INTERGRANULAR STRESS CORROSION CRACKING OF AUSTENITIC STAINLESS STEEL IN STEAM-WATER MIXTURE

Yu.D.Goncharenko, V.A.Kazakov, V.K.Shamardin, A.M.Pechyorin, G.V.Filyakin, Z.Ye.Ostrovsky
Federal State Unitary Enterprise
"State Scientific Center of Russian Federation Research Institute of Atomic Reactors"
Dimitrovgrad, Ulyanovsk region, Russia

Ціль запропонованої роботи – отримати результати для того, щоб зробити питомий внесок у розуміння механізму радіаційного обумовленного міжзеренного корозійного розтріскування аустенітних нержавіючих сталей.

Цель предложенной работы – получение новых результатов для того, чтобы внести конструктивный вклад в понимание механизма радиационно-обусловленного межзеренного коррозионного растрескивания аустенитных сталей.

The objective is to obtain the new results in order to make a constructive contribution into understanding of the mechanism of austenitic stainless steels (ASS) irradiation-assisted intergranular stress corrosion cracking (IAISCC).

INTRODUCTION

Susceptibility of austenitic stainless steels (ASS) to stress corrosion cracking (SCC), which is of intergranular type in most cases (ISCC), is one of the important problems of their usage as in-vessel devices components (IVDC) of nuclear and fusion reactors in water-steam environment [1-4]. This fact is caused by chromium depletion of the boundaries and their adjoining zones in the sensitive areas near the welded joints as a result of precipitation of chromium carbides such as $Me_{23}C_6$ and/or Me_6C [1,2].

Neutron irradiation facilitates the SCC propagation due to the radiation-induced segregation and depletion processes at the interphase surfaces. Moreover, the specific mechanisms of sulfur release from MnS sulfides due to nuclear transformation of ^{54}Mn into ^{56}Fe, cascade intermixing on the sulfide surface and advanced penetration of manganese deep into the metal because of inverse Kirkendall effect [5] have been proposed for the irradiation conditions. The processes are followed by etching of grain boundaries with sulfur, fluorine and chlorine that are dangerous elements from the corrosion point of view.

In-vessel devices components of 35 BWR-type German reactors made of austenitic stainless steel [6] were subjected to examination not long ago. Cracks caused by ISCC were discovered in IVDC of 24 reactors. They were 390mm in length as a maximum and 25…30mm in depth. All cracks were discovered in the areas of residual stress caused by cold surface hardening in machining and welding.

The real IVDC that have been operated for a long time are the most informative material for SCC investigation under neutron irradiation. The external 0X18H10T ASS tube of VK-50 control assembly was chosen as the subject of examination in this case. It was damaged in the welded joint area after 30 years of operation during the scheduled replacement.

The objective– to obtain new results in order to make a constructive contribution into understanding of the mechanism of ASS irradiation-assisted intergranular stress corrosion cracking (IAISCC).

1. MATERIAL, SPECIMENS, OPERATING CONDITIONS

The chemical composition of the tube (∅152×3 mm) made of 0X18H10T is as follows: C ≤ 0.08; Si ≤ 0.8; Mn ≤ 2.0; Cr = 17.0…19.0; Ni = 9.0…11.0; Ti = 0.4…0.7; S ≤ 0.02; P ≤ 0.035; Cu ≤ 0.3 mass%. The tube was operated during 271 500 hours at a temperature of 285, 264 and 250^{O}C. The tube was damaged in the welded joint area at a distance of 10-20mm from the melting zone of the welded joint. The neutron fluence in the place of fracture was $2.2\cdot 10^{21}$ n/cm^2 (E > 0.5 MeV) or $3.0\cdot 10^{21}$ n/cm^2 (E > 0.1 MeV). The chemical composition of the steam-water mixture was the following: water hardness–1.2 μmole/dm^3; pH – 6.0…6.2; Fe^{3+} – 0.012 mg/dm^3; Cl^- – ≤ 0.05 mg/dm^3; Cu^{2+} – 0.009…0.03 mg/dm^3; nitric oxide NO – 0.011…0.03 ml/dm^3; Zn^{2+} – 0.01…0.04 mg/dm^3; specific electric conductivity – 0.18…0.2 μS/cm.

A wrapper was operated under alternate cooling with subboiling water and steam-water mixture at the saturation temperature in the place of fracture. The visual inspection of the fracture place reveled cracks

both in transverse and longitudinal directions. Some cracks were 120…140mm in length.

2. RESULTS OF EXPERIMENT

2.1. METALLOGRAPHY, FRACTOGRAPHY, MECHANICAL PROPERTIES

Fig.1 demonstrates the typical view of the fracture surface and cracks. It was noticed that cracks grow along the grain boundary only and they grow in both transverse and longitudinal directions. The fracture exhibits brittle, grain-boundary character although there are traces of fresh cleavages caused by transcrystalline fracture in the fine areas that adjoin the grain boundaries. Flat tensile specimens were cut out form the tube section adjacent to the place of fracture using the electro-erosion technique. A test portion of specimens was 15×3×3 mm in size. The yield stress of irradiated specimen increased by a factor of two at 20^{O}C when compared to the initial state and reached 850…950 MPa, the uniform relative elongation δ_r came to 12… 25% and the total one δ_t comprised 26…38%. δ_r fell to 0.8…4% and δ_t – to 14…15% at a test temperature of 280^{O}C. The material damaged with the formation of developed neck in both cases and the fracture exhibited transcrystalline character.

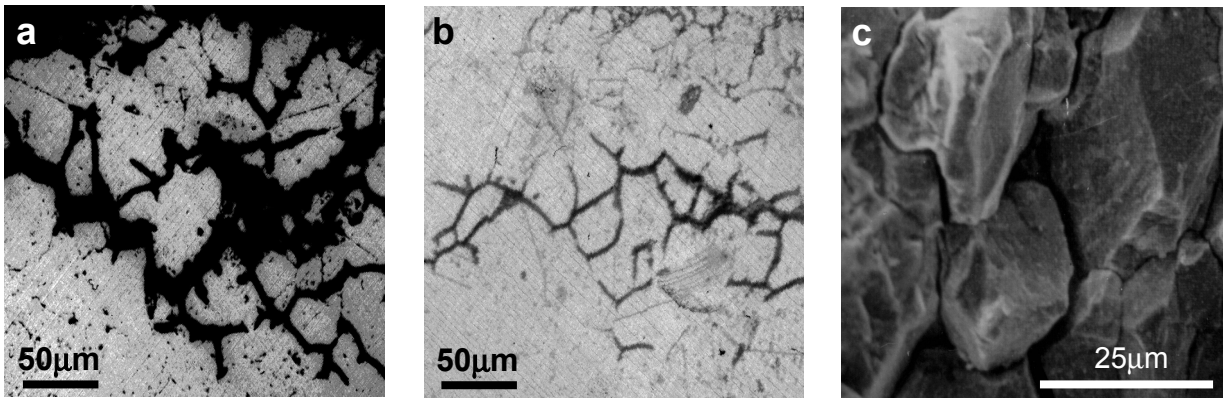

Fig.1. Fracture surface (a,c) and typical view of cracks (b). Optical metallography (a, b); scanning electron microscope investigation (c)

2.2. TRANSMISSION ELECTRON MICROSCOPE INVESTIGATION

As illustrated in Fig.2**,** segregation of secondary phases that range in size from several tens to several hundreds of nanometers and align themselves in the main along the grain boundaries and in the near-boundaries areas (Fig.2a, b) takes place during the 0X18H10T steel irradiation. Their chemical composition is as follows: 37…46 Fe, 11…15Cr, 32… 45Ti, 5…6Ni, atomic%. Based on the structure, these precipitates are likely to be $Me_{23}C_6$ or Me_6C type carbides. The large precipitate in Fig.2c is the titanium carbide TiC. Fine-dyspersated precipitates of a round shape are discovered in the grain body. They are assumed to be the G-phase. Their medium size is about 8 nanometers and density constitutes $5\cdot 10^{15}$ cm^{-3}. The average diameter of dislocation loops was 9 nanometers, their density comprised $1.4\cdot 10^{16}$ cm^{-3}.

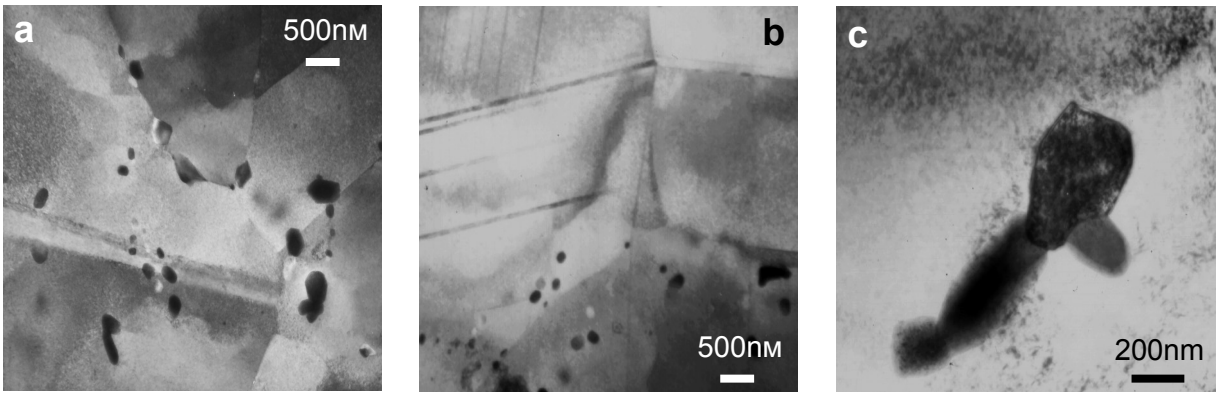

Fig.2. The tube material microstructure after irradiation. Transmission electron microscope investigation

2.3. HYDROGEN ANALYSIS

The hydrogen content was analyzed using a etalon-free spectral-isotopic method. Hydrogen constitutes 0.003 mass% in the X18H10T steel in the initial state. The hydrogen content increased insignificantly and made up 0.0045 mass% after operation. For comparison, the hydrogen content in X18H10T increased nine times in the temperature range 300-395^{O}C and at a neutron fluence of $1\cdot 10^{22} \div 1.7\cdot 10^{23}$ n/cm^2 after operation in the BOR-60 reactor.

2.4. AUGER SPECTROSCOPY

A fresh fragment of the fracture surface to be 2×2 ×0,3 mm in size was used for examination. The primary electron beam with a diameter of 3μm was focused into a raster to light a fracture section to be ~ 200×200 μm in size in order to obtain a surface- average values for concentrations of different elements. A multiple ion etching of the surface under investigation was carried out after the Auger spectra recording (10…12 atomic layers) from the fracture surface to analyze the elemental composition in depth. The thickness of the remote layer was calculated based on the etching rate that is approximately equal to 20 angstorm per second.

As illustrated in Fig.3a, chromium and nickel are fully absent but titanium is present in large quantities. Its content is 60 times greater than in the matrix. The changed layer depth varies between 0.2 and 1.2 μm. The carbon content falls to the level of initial state at ~1.2μ m, whereas the high level of oxygen is kept constant and makes up about 40 atomic% at a depth of 1 μm (Fig.3b). The depth of sulfur and chlorine layers makes up about 0.2 and 0.4 μm respectively. It is about 1 μm for copper. The calcium content decreases sharply in 0.2 μm thick layer but it disappears completely at a depth of 1 μm (Fig.3c).

a d c

Fig.3. Content of the primary alloying elements (a, except for light and impurity ones), oxygen, carbon (b), as well as sulfur, chlorine, copper and calcium (c) against the fracture surface distance in the irradiated steel

In order to obtain data on uniform or non-uniform distribution of different elements on the fracture surface we recorded series of elemental images at an accelerating voltage of 3 and 9kV. Fig.4 shows the images of the fracture surface for one of the grains that is arranged in the center of each picture. As shown in Fig.4a, chlorine is distributed uniformly. Contrary to chlorine sulfur is found in aggregations to be 5…6 μm in size (Fig.4b). This fact is well visible at lesser magnifications and accelerating voltage of 3 kV (Fig.4c). As a rule, the sulfur aggregations are characterized by higher concentration of iron (Fig.4e), chromium (Fig.4h) and nickel as well. The sulfur aggregations appear to be the complex sulfide compounds, which incorporate iron, chromium and nickel.

Copper is distributed by separate aggregations along the boundaries of grain under examination (Fig.4d). Higher concentration of copper has been noted in several places around the periphery of a facet but it is absent on its surface. A map of carbon distribution (Fig.4g) those Auger peak is the most intensive one is much the same as the image of the fracture surface in absorbed or secondary electrons (Fig.4i) according to the topographic tinctures.

Any specific carbon aggregations are absent but there are regions of its lower concentration where the oxygen content is higher (Fig.4f, g). Higher oxygen content in the right lower part of the facet (Fig.4f) is followed by higher nickel concentration and slightly increased chromium concentration (Fig.4h).

3. DISCUSSION OF RESULTS

The following conclusions can be drawn according to the obtained results:

- Fracture occurs mainly along the grain boundaries.
- Ti segregates on the grain boundaries, but Cr and Ni deplete them.

- Chlorine, sulfur and copper that are dangerous elements from the corrosion point of view, are available on the fracture surface.

The thickness of the segregation layer on the fracture surface is about 1…1.5 μm; in any case after ion etching at a depth of ~ 3 μm segregation phenomena disappear practically (Fig.5).

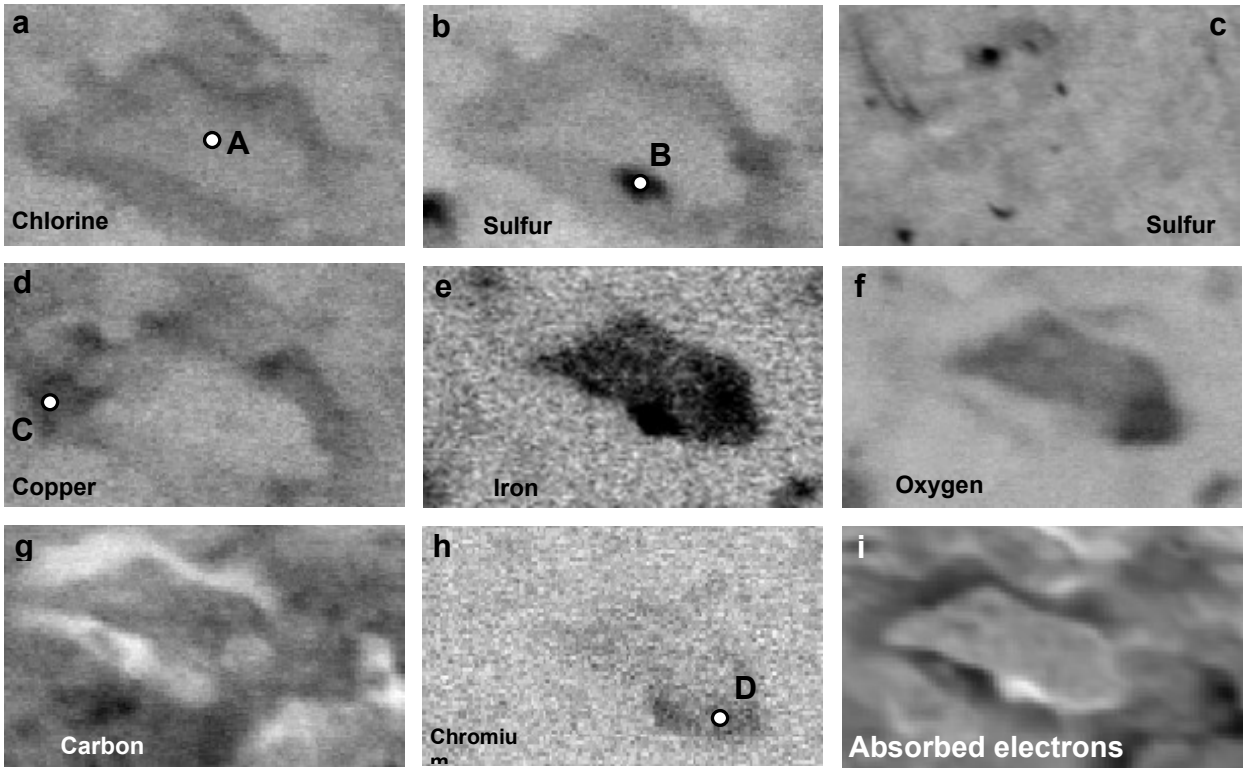

Fig 4. Images for distribution of elements on the irradiated steel fracture surface (a,b,d-i – 1400^{u}; c – 400^{u}; A,B,C,D – places of local elemental composition analysis)

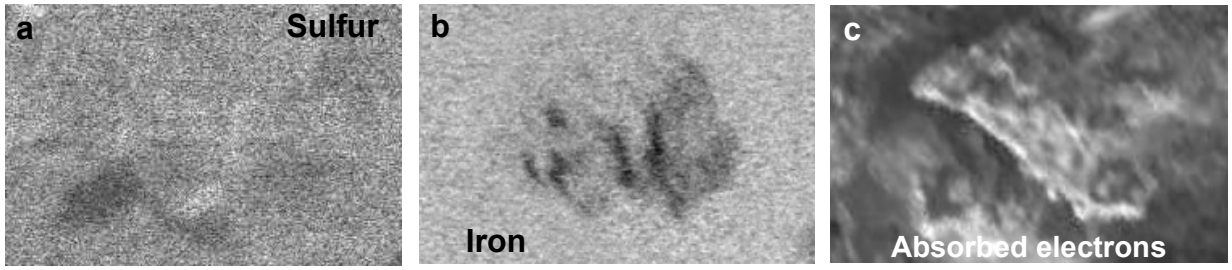

Fig.5. Images of sulfur and iron distributions on the fracture surface of the irradiated steel at a depth of 3 μm after ion etching. 1500^{x}

Table 1

Local elemental composition of the fracture surface

Ele-ment	Content, atomic %				
	«A»	«B»	«C»	«D»	Raster
Fe	4.0	12.2	1.7	7.4	2.4
Cr	0.5	2.8	0.8	1.6	0.6
Ni	3.8	5.1	1.4	6.5	0.3
Ti	1.0	0.6	0.6	1.2	0
C	75.9	61.7	82.5	47.0	91.5
O	13.0	13.1	6.3	30.8	3.9
Cl	0.5	0.4	0.6	0.3	0.3
S	0.4	2.7	0.1	0	0.4
Cu	0.8	1.4	6.2	3.0	0.5
Ca	0	0	0	2.3	0

3.1. DISTRIBUTION OF ELEMENTS ON THE FRACTURE SURFACE

Images provide the qualitative representation of element distribution. But the quantitative information can be gained from the local elemental composition analysis at different points when the diameter of the electron probe is 0.1…0.3 μm (in our case it is performed at points "A – D», Fig.4, Table 1). For comparison purposes the Table includes the results of integral analysis of the elemental composition in a raster of 200×200 μm. The facet under examination entered its area. The results of local measurements agree well with the quantitative information obtained from the maps. As the Table indicates chlorine is the only element that is distributed on the fracture surface rather uniformly. The

concentration of other elements varies within rather wide limits.

3.2. SUMMARY OF FACTORS IMPORTANT FOR IAISCC OF ASS

Literature data [1-7] and obtained results enable us to define three groups of factors: 1) principal, 2) determining and 3) contiguous.

Principal factors: 1) Tensile stress. Cracks were observed only in the welded joint area in the upper part of the tube. In accordance with data [4] tensile stress in this area may reach 300MPa. In the base metal in the lower part of the tube, where neutron fluence was higher, cracks were not observed. Therefore, it is logically to assume that tensile stresses in IAISCC dominate over radiation-induced segregation/depletion processes. 2) Sensitivity. Heating of the area near welded joint up to 550…800^{O}C during welding leads to precipitation of large $Me_{23}C_6$ and/or Me_6C type carbides along the grain boundaries and in the near-boundaries areas. The size of these carbides is several hundred nanometers (Fig.2), their chemical composition is as follows: Cr-13%, Fe-42%, Ti-39% and Ni-6%.

This is one of the sources of grain boundaries depletion in chromium. The next depletion source is pure thermal low-temperature sensitivity in the temperature range 250…350^{O}C. As the evalution shows, the time necessary for this process is 12 years at 285^{O}C [4].

This time period is in two and a half lesser than the tube operation time. The third and probably the most powerful source of grain boundaries depletion in chromium is the radiation-induced one. It seems to combine 3 processes: a) growth of the existing carbides; b) radiation depletion of grain boundaries in chromium; c) precipitation of fine-dispersed phases containing chromium.

Table 2

Radiation effect on the change of chemical composition of SS 304 grain body and near-boundaries areas at 300ºC [7]

Element	Energy dispersion analysis, TEM investigations, mass%			Auger-electron microscopy investigation, atomic%			
	Initial state		5· 10^{21} n/cm^2, grain boundaries	Initial state		5· 10^{21} н/см^2	
	Grain body	Grain boundaries		Grain body	Grain boundaries	Grain body	Grain boundaries
Fe	score	62-64	61	69.39	74.9	68.4	60.6
Cr	18.54	24-25	16	19.58	16.4	18.7	14.2
Ni	8.28	9	15-16	7.75	7.8	8.43	14.1
Mo	0.32	1.7-1.9	1	0.18	Not analyzed	1.53	0.2
Mn	1.52	Not analyzed	Not analyzed	Not analyzed	Not analyzed	Not analyzed	Not analyzed
Si	0.55	1	4.2-4.5	1.08	Not analyzed	1.25	8.3
C	0.069	Not analyzed	Not analyzed	Not analyzed	Not analyzed	Not analyzed	Not analyzed
P	0.023	0.8	1.1	0.04	0.7	0.06	1.9
S	0.021	Not analyzed	Not analyzed	Not analyzed	Not analyzed	Not analyzed	Not analyzed

Paper [7] presents the analysis of segregation processes at the grain boundaries of steel 304 before and after irradiation at 300^{O}C (Table 2). The Table indicates that chromium and silicon segregate noticeably but molybdenum and phosphorus segregate especially strong at the grain boundaries in the initial state according to the results of energy dispersion analysis (EDA). The results of Auger-electron microscopy investigation didn't prove chromium segregation. The depletion of grain boundaries in chromium, molybdenum and their enrichment in nickel, phosphorus and especially strong in silicon was revealed after irradiation according to the EDA results. As for irradiated state the results of EDA and Auger-spectroscopy agree qualitatively but they correlate better for molybdenum, silicon and phosphorous that are subjected to Auger-electron microscopy investigations. The results of these examinations with regard to chromium agree with the results of the given paper principally but the effect is much stronger. But they are in direct opposition to nickel: as for nickel the depletion of grain boundaries up to zero is revealed in our case, and in work [7] the enrichment of grain boundaries in nickel is observed.

Therefore, the conclusion may be drawn that radiation-induced segregation processes at the grain boundaries present the second important factor in IAISCC phenomenon.

Determining factors: 1) High oxygen concentration in the water-steam mixture, which may reach 0.2…0.5 mg/l in water and up to 20-50 mg/l in steam [1,2] as a result of radiolysis, facilitates the increase of metal dissolution rate at the intergranular channels tops. 2) Chlorine precipitation at the boundaries. Coolant is probably the major chlorine source. The capability of chlorine to be accumulated at the steam/water interface facilitates the process of chloride cracking even if the chlorine-ion content is <0.1 mg/l. The additional, although not so strong chloride source, is transmutation of sulfur into chlorine and possible chlorine release from decaying manganese sulphides [5]. 3) Sulfur poisoning of grains boundaries. Sulfur, acting as poison during electrochemical processes and decreasing the rate of repassivation after oxide film rupture, facilitates the development of

local anode processes. Coolant and sulfides unbound sulfur are probably the main sulfur source. The additional source of sulfur can be radiation-induced MnS sulfide decay as shown in work [5]. In some places of the fracture surface sulfur content reaches 2.7%. *4)* Copper effect. It is known [1,2] that bivalent copper ions facilitate chloride corrosion cracking. Besides ~0.3% copper present in steel it was also present in coolant (up to 0.03 mg/l). It was enough for copper concentration reaching 6.2% on the fracture surface and in the near boundary areas.

Contiguous factors: *1)* enrichment of grain boundaries with carbon and oxygen, the content of which reaches 50 atomic %. 2*)* Effect of steam/water separation boundary. The alternative cooling with water underheated by 5-7ºC up to a boiling temperature and with water-steam mixture was observed at the investigated tube section during the reactor operation. Therefore, the section was located at the steam/water interface that is characterized by the greatest danger for corrosion cracking resulting from chlorides accumulation at multiple dryouts and facilitation of oxygen access.

3.3 ASS IAISCC MECHANISM

The analysis of literature and obtained results without any claim to originality enables us to assume the ASS IAISCC mechanism in the following way.

At the primary stage, when cracks, pores and other defects are present on the metal oxide film the rate of general corrosion process is relatively high. The generated slightly insoluble corrosion products gradually heal the defects of oxide film on the grains and decrease the area and number of anode sections. The effect of anodes gradually propagates to the sensitive grain boundaries. This period is considered as incubation period [1,2].

Then the process proceeds at a low rate suitable for the anode dissolution rate in passive state. The maximum rate is observed in the areas with minimum chromium concentration and as a result of it the corrosion has a nodular character. As the intergranular cracks propagate, the corrosion products obstruct the access of fresh portions of water/steam to the anode sections and removal of metal ions in the opposite direction. Moreover the access of cathode depolarizer (oxygen) is obstructed. As a result, the cathode process is transferred onto the walls of intergranular channels close to the surface [1,2].

Gradually the poisoning process of grain boundaries with sulfur and chloride released from coolant and from radioactive decay of MnS manganese sulfides becomes stronger. Copper precipitation begins on the surfaces of the generated intergranular cracks. Complex aggregations on the basis of sulfur and copper are being generated. They consist of iron, chromium, nickel, carbon and oxygen also.

The effect of radiation-induced processes of grain boundaries depletion in chromium and nickel with their simultaneous enrichment in titanium, phosphorus and silicon increases. The chemical composition of boundary areas differs more and more from the matrix chemical composition. Under the effect of the residual tensile welded stresses the intergranular crack nuclei grow in width and length. At the final stage they reach the length of some tens of millimeters and form one main cross crack. The process of intergranular corrosion cracking results into the transverse fracture of the tube.

4. CONCLUSIONS

X18H10T ASS tube was subjected to elementary and structural analysis after 30 years of operation in VK-50 at a temperature of 285…250^{O}C in the steam/water mixture. The tube was fractured in the welded joint area where the neutron flux was $3.0\cdot 10^{21}$ n/cm^2 (E>0.1 MeV). The following conclusions can be drawn according to the obtained results:

1. The tube was fractured along the main cross crack as a result of intergranular corrosion cracking in the welded joint area where the generation of crack network to be 140 mm in length was revealed.

2. The mechanical properties of the tube in the base metal adjacent zone remained high but the transcrystalline corrosion took place at high necking of specimens. The transmission electron microscope investigations revealed the precipitation of $Me_{23}C_6$ and/or Me_6C carbides, TiC titanium carbides to be several hundreds nanometers in size, G-phase of the medium size 8 μm as well as generation of dislocation loops of the average diameter 9μm.

3. The principal factors of the intergranular corrosion cracking are: 1) residual tensile welded stresses; 2) sensitization of austenite in the welded joint area during welding; 3) radiation-induced low-temperature sensitization in irradiation; 4) radiation-induced segregation and depletion processes at the grain boundaries.

4. Chemical composition of grains and their adjacent areas to be 1μm in width after irradiation had nothing in common with the initial chemical composition of matrix. They depleted in chromium and nickel greatly and enriched in titanium. As a rule the width of zones is different for different elements and varies between 0.2 and 1 μm.

5. The wide application of Auger-spectroscopy followed by construction of the elemental maps of the fracture surface, raster and point elemental spectra allowed us to link all data together with the help of quantitative analysis of the elemental and structural peculiarities at the grains boundaries.

REFERENCES

1. I.I. Vasilenko & al. *Corrosion cracking of steels* K.:, «Naukova Dumka», 1977.

2. V.P. Pogodin & al. *Intergranular corrosion and corrosion cracking of stainless steels in water environment* M.:, Atomizdat, 1970.

3. G.G. Ulig, R.U. Revi. *Corrosion and corrosion control. Introduction into corrosion science and technology*. L.: Chemistry, 1989.

4. A.A. Nazarov. *Susceptibility of steel to intergranular corrosion and current methods of its evaluation.//* Review. «Prometey». 1991.

5. F.A.Garner, L.R.Greenwood, H.M.Chung. Irradiation-induced instability of MnS precipitates and its possible contribution to IASCC in light water reactors. //*Proc. of 8-th Internat. Sympos. on Environm. Degra-*

dation of Materials in Nuclear Power Systems–Water Reactors. August 10…14, p.857-860.
6. O.Wachten, U.Wesseling, J.Bruns, R.Kilian, A.Roth. Crack initiation in the Nb-stabilized austenitic steel (A347) in the core shroud and top and core guide of a German boiling water reactor – description of the extent of the damage and explanation of its causes. //*Proc. of 8-th Internat. Sympos. on Environm. Degradation of Materials in Nuclear Power Systems–Water Reactors. August 10…14*, 1997, USA, Florida, p. 725-733.
7. J.F.Williams, P.Spellward, J.Walmsley, T.R.Mager, M.Koyama, H.Mimaki, I.Suzuki. Microstructural effects in austenitic stainless steel materials irradiated in a pressurized water reactor. //*Proc. of 8-th Internat. Sympos. on Environm. Degradation of Materials in Nuclear Power Systems–Water Reactors. August 10… 14*, 1997, USA, Florida, Refer, p. 812-822